

Kagome Lattice Formation through Preliminary Structures in Colloidal Heteroepitaxy

メタデータ	言語: English 出版者: 公開日: 2025-05-28 キーワード: 作成者: 佐藤 正英, Jun Nozawa メールアドレス: 所属:
URL	https://doi.org/10.24517/0002002810

This work is licensed under a Creative Commons Attribution-NonCommercial-ShareAlike 4.0 International License.



Kagome Lattice Formation Through Preliminary Structures in Colloidal Heteroepitaxy

Masahide Sato^{*,†} and Jun Nozawa[‡]

[†]*Emerging Media Initiative, Kanazawa University, Kanazawa 920-1192, Japan*

[‡]*Institute for Materials Research, Tohoku University, 2-1-1 Katahira, Aoba-ku, Sendai 980-8577, Japan*

E-mail: msato002@staff.kanazawa-u.ac.jp

Abstract

Brownian dynamics simulations were conducted to investigate the formation of a kagome lattice in the first epitaxial layer during colloidal heteroepitaxy. When the epitaxial particles were smaller than the substrate particles, and the interactions were predominantly governed by the depletion force, a kagome lattice structure was successfully formed in the first epitaxial layer when the epitaxial particles were a specific size. The formation process of the kagome lattice in the first layer was analyzed in detail. Initially, the epitaxial particles adhered to positions where they interacted with three substrate particles. When the density of epitaxial particles on the substrate increased by sedimentation, the epitaxial particles changed locations to attach to the sites where they interacted with one or two substrate particles, and a hexagonal structure formed. Subsequently, particles interacting with only one substrate particle detached from the substrate, resulting in the formation of a kagome lattice.

Introduction

Colloidal particles have a size that is comparable to the wavelength of visible light, which makes them promising materials for use as photonic crystals.¹⁻⁴ Photonic crystals with open structures like the diamond structure exhibit a large photonic band gap because the periodicity of the colloidal crystal lattice can strongly influence light propagation. Photonic crystals with another open structure, the kagome structure, also have unique optical and mechanical properties.^{5,6} Consequently, numerous research groups have tried to develop efficient methods to fabricate colloidal crystals with precisely controlled structures for use in photonic devices. The structure of colloidal crystals may be controlled by adding patches.⁷⁻¹³ Desired structures can be formed when the number, size, shape, and position of these patches are varied appropriately. Preparing precursors as building blocks is another useful method to generate complex structures.¹⁴⁻¹⁷

Colloidal epitaxy, in which colloidal crystals grow aligned with the crystal planes of the underlying substrate, is also an effective method for generating target fine structures.¹⁸⁻³¹ Nozawa and co-workers have fabricated various structures using colloidal heteroepitaxy.³²⁻³⁴ Performing Monte Carlo³⁵ and Brownian dynamics simulations³⁶ for systems with the short-range interaction mimicking the depletion force, we systematically investigated how the ratio of the size of epitaxial particles to that of substrate particles is related to the structure of the first epitaxial layer in heteroepitaxial growth. Complex structures, including those observed in an experiment,³³ were obtained by selecting a specific ratio of the size of epitaxial particles to the size of substrate particles.

Recently, we³⁴ experimentally found that multilayer kagome lattices were generated in colloidal heteroepitaxy even when simple spherical colloidal particles were used. In this experiment, we observed the formation process of the first epitaxial layer with a kagome lattice in detail and found that the kagome lattice was produced after honeycomb lattice formation followed by the generation of a hexagonal lattice. A kagome lattice can form when patchy or non-spherical particles such as those with an elliptic³⁷ or rhombus³⁸ shape are used. Even

for simple spherical particles, a kagome lattice can form when particles interact with complex interaction potentials.^{39,40} However, in our experiment,³⁴ the particles were spherical and the depletion force, which had a simple form, appeared to be the predominant interaction between particles. Monte Carlo³⁵ and Brownian dynamics simulations³⁶ are useful to investigate the formation of various epitaxial layers. On the basis of these studies, here we conduct Brownian dynamics simulations to examine whether the kagome lattice observed in our experiment³⁴ forms through colloidal heteroepitaxial growth. Final structures may be obtained in Monte Carlo simulations. However, in this study we focus on the time evolution of the assembly process, for which Brownian Dynamics simulations are more appropriate. Thus, we conduct Brownian Dynamics simulations.

Methods

An interaction potential that included features of the Asakura–Oosawa (AO) potential^{41,42} was used in Brownian dynamics simulations. In experiments,^{32–34} colloidal particles moved downwards in solution, including polymer solutions, driven by gravity. Because the colloidal particles were exposed to viscous resistance and thermal noise, their motion in a solution can be described by a Langevin equation. When the viscosity of the solution is high, the inertia term in the Langevin equation can be ignored. The equation of motion of the i th particle is given by⁴³

$$\frac{d\mathbf{r}_i}{dt} = \frac{1}{\xi_i} (\mathbf{f}_i + \mathbf{f}_i^g + \mathbf{f}_i^B), \quad (1)$$

where t is time, \mathbf{r}_i is the position of the i th particle, ξ_i is the friction coefficient acting on the i th particle. \mathbf{f}_i , \mathbf{f}_i^g , and \mathbf{f}_i^B are the forces from other particles, gravity, and thermal noise, respectively. When the interaction potential between the i th and j th particles is given by $U(r_{ij})$, where $r_{ij} = |\mathbf{r}_{ij}| = |\mathbf{r}_i - \mathbf{r}_j|$ is the distance between the two particles, \mathbf{f}_i is expressed by $-\nabla U(r_{ij})$. $f_{i,x}^B(t)$, $f_{i,y}^B(t)$, and $f_{i,z}^B(t)$, which are the x , y and z components of

\mathbf{f}_i^{B} , respectively, satisfy the following relationships;

$$\langle f_{i,x}^{\text{B}}(t) \rangle = \langle f_{i,y}^{\text{B}}(t) \rangle = \langle f_{i,z}^{\text{B}}(t) \rangle = 0, \quad (2)$$

$$\langle f_{i,x}^{\text{B}}(t) f_{i,x}^{\text{B}}(t') \rangle = \langle f_{i,y}^{\text{B}}(t) f_{i,y}^{\text{B}}(t') \rangle = \langle f_{i,z}^{\text{B}}(t) f_{i,z}^{\text{B}}(t') \rangle = 2\xi_i k_{\text{B}} T \delta(t - t'), \quad (3)$$

where k_{B} is the Boltzmann constant, T is temperature, and angle brackets denote the ensemble average. For a short time interval Δt , Eq. (1) can be differentiated as⁴³

$$\mathbf{r}_i(t + \Delta t) = \mathbf{r}_i(t) - \frac{1}{\xi_i} \sum_{i \neq j} \frac{dU(r_{ij})}{dr_{ij}} \frac{\mathbf{r}_{ij}}{r_{ij}} \Delta t - \frac{4\pi R_i^3}{3\xi_i} \Delta \rho g \Delta t \mathbf{e}_z + \Delta \mathbf{r}_i^{\text{B}}, \quad (4)$$

where R_i is the radius of the i th particle. The third term on the right hand side of Eq. (4) shows the gravitational sedimentation of particles toward the $-z$ -direction. $\Delta \rho$ is the density difference between the particle and solution. g is the gravitational acceleration, and \mathbf{e}_z is the normal vector in the z -direction. $\Delta \mathbf{r}_i^{\text{B}}$ represents the displacement caused by thermal fluctuations. Δx_i^{B} , Δy_i^{B} , and Δz_i^{B} are the x , y , and z components of $\Delta \mathbf{r}_i^{\text{B}}$, respectively, which satisfy the following constraints;

$$\langle \Delta x_i^{\text{B}} \rangle = \langle \Delta y_i^{\text{B}} \rangle = \langle \Delta z_i^{\text{B}} \rangle = 0, \quad (5)$$

$$\langle (\Delta x_i^{\text{B}})^2 \rangle = \langle (\Delta y_i^{\text{B}})^2 \rangle = \langle (\Delta z_i^{\text{B}})^2 \rangle = \frac{2k_{\text{B}} T}{\xi_i} \Delta t. \quad (6)$$

In experiments,^{32,33,45,46} the main attractive force is the depletion force, for the potential of which is often described using the AO potential.^{41,42} The AO potential is a short-range interaction; an attractive interaction occurs when the distance between the particle surfaces is shorter than the polymer's radius of gyration R_{g} . For the interaction between the i th and j th particles, the potential reaches a minimum when the two particles come into contact; that is, when the distance between them is $R_i + R_j$. When R_i and R_j are sufficiently larger than R_{g} , the potential depth is proportional to $R_{\text{g}}^2 R_i R_j / (R_i + R_j)$. If the AO potential is used, Equation (4) does not apply well because there is a hard-core repulsive interaction.

Thus, the Morse potential,⁴⁷ which has a steep repulsion and short-range attraction, was used in place of the AO potential. This is because the formation of various structures observed in experiments^{32,33} gas previously been explained using the Morse potential. The potential minimum of the Morse potential was proportional to $R_i R_j / (R_i + R_j)$ and located at a distance $(R_i + R_j)$. The Morse potential is given by

$$U(r_{ij}) = U_0(R_i, R_j) \left[1 - \exp\left(-\frac{r - R_e}{2R_g}\right) \right]^2 - U_0(R_i, R_j), \quad (7)$$

where $R_e = R_i + R_j$. We can control the interaction range by changing the value of R_g . The depth of the potential $U_0(R_i, R_j)$ is given by

$$U_0(R_i, R_j) = \frac{4AR_i R_j}{(R_i + R_j)}. \quad (8)$$

where A is a constant. During colloidal epitaxy, hydrodynamic interactions and the variation of colloid diffusivity near the substrate may play important roles. However, for simplicity, we neglect these effects in our model and focus on whether the Kagome lattice can be created solely by a simple depletion potential.

The simulations were conducted in cuboidal systems with dimensions of $L_x \times L_y \times L_z$, where L_x , L_y , and L_z are the lengths of the simulation box in the x -, y -, and z -directions, respectively. Periodic boundary conditions were applied in the x and y directions. A hard wall was placed at $z = L_z$ to prevent particles from leaving the system. The epitaxial particles were treated as hard spheres of radius R_{epi} . N_{sub} substrate particles with a radius of R_{sub} were located on the $z = 0$ plane. Because the motion of the substrate particles can be ignored in experiments,^{33,34} the particles were fixed with a close-packed hexagonal structure with a lattice constant of $2R_{\text{sub}}$. Initially, N_{epi} epitaxial particles with radius R_{epi} were randomly distributed within the cuboidal system. Then, they were moved according to Eq. (4).

In the simulations, the scaled variables $\tilde{\mathbf{r}}_i = \mathbf{r}_i / (2R_{\text{sub}})$ and $\tilde{t} = t / t_s$ were introduced.

By using $\xi_0 = \xi_i R_{\text{sub}}/R_{\text{epi}}$, which is independent of R_i because ξ_i is proportional to R_i , t_s is given by $2\xi_0 R_{\text{sub}}^2/k_B T$. L_y and L_x were determined on the basis of the hexagonal structure of the substrate particles, and L_z was set to achieve a volume fraction of particles ρ . In our simulation, we used $N_{\text{sub}} = 36$, $N_{\text{epi}} = 900$, and $\rho = 0.1\text{--}0.3$. The normalized time increment $\Delta t = 5.0 \times 10^{-5}$ was employed in Eq. (4). The scaled gravitational force is given by $\alpha(R_{\text{epi}}/R_{\text{sub}})^3 \mathbf{e}_z$, where $\alpha = 4\pi R_{\text{sub}}^4 g \Delta\rho/3k_B T$. Because the experiment³³ was conducted with $\Delta\rho \simeq 50 \text{ kg/m}^3$ for polystyrene with a typical value of $R_{\text{sub}} = 5.0 \times 10^{-7} \text{ m}$ at room temperature, α was estimated to be about 3×10^{-2} . Thus, we used this value in our simulation. In our model, the effect of gravity on the polymers in solution was neglected because the polymers that we considered were much smaller and lighter than the epitaxial particles. Hereafter, although the tilde have been omitted from \tilde{r} and \tilde{t} , time and length are scaled unless otherwise specified.

Results and discussion

In our previous studies,^{35,36} the ratio $R_{\text{epi}}/R_{\text{sub}}$ required to generate the desired structure was consistently about 1.1 times larger than the values reported in experiments.^{32,33} In a recent experiment,³⁴ a kagome structure was observed when $R_{\text{epi}}/R_{\text{sub}} = 586/1338 = 0.438$. On the basis of this observation, our model predicted the formation of the kagome lattice at $R_{\text{epi}}/R_{\text{sub}} = 0.48$. Thus, we performed the simulations using particles with $0.47 \leq R_{\text{epi}}/R_{\text{sub}} \leq 0.49$ and investigated the dependence of the formation of a kagome lattice on the size of epitaxial particles.

A typical snapshot of a kagome lattice. First, the simulation was conducted with $R_{\text{epi}}/R_{\text{sub}} = 0.48$, $A/(2R_{\text{sub}}k_B T) = 5.6$, and $\rho = 0.02$. Under these conditions, the potential minima for the interaction between an epitaxial particle and substrate particle $U_0(R_{\text{epi}}, R_{\text{sub}})$, and between epitaxial particles $U_0(R_{\text{epi}}, R_{\text{epi}})$, were 3.63 and 2.69, respectively. Thus, the interaction between an epitaxial particle and substrate particle was stronger than that be-

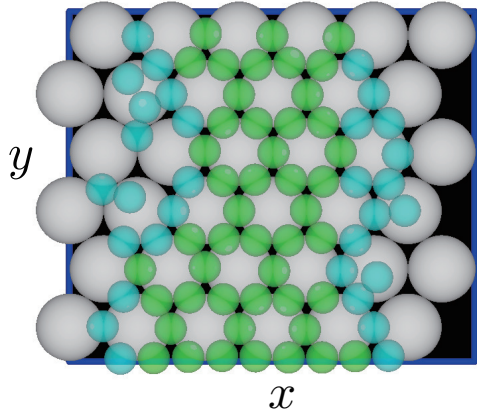


Figure 1: Snapshot of the epitaxial layer exhibiting a kagome lattice. The simulation parameters were as follows: $N_{\text{sub}} = 36$, $N_{\text{epi}} = 900$, $\rho = 0.02$, and $2R_{\text{sub}}A/k_{\text{B}}T = 5.6$. The simulation was performed up to $t = 2 \times 10^3$ with $\Delta t = 5.0 \times 10^{-6}$. Substrate particles are represented in white, epitaxial particles forming the kagome lattice are shown in green, and other epitaxial particles on the substrate are depicted in cyan.

tween epitaxial particles. However, both interactions were sufficiently larger than thermal fluctuations. Figure 1 shows a snapshot of the first epitaxial layer at $t = 2 \times 10^3$. When the distance between an epitaxial particle and substrate particle exceeds $r_c = 0.1$, the interaction is considered negligibly weak and these epitaxial particles are not drawn. In Fig. 1, green particles represent those forming in the Kagome lattice, and cyan particles represent other epitaxial particles attached to substrate particles.

Criteria for identifying particles included in the kagome lattice. When the k th particle attached to the substrate particles is part of the kagome lattice, its local bond orientational order parameter, defined as

$$\phi_6(k) = \frac{1}{N} \left| \sum_l^N \exp(6i\theta_{kl}) \right|, \quad (9)$$

is unity. In the calculation of $\phi_6(k)$, particles were considered neighbors when the distance between them satisfied $|\mathbf{r}_{kl}| \leq 3r_c$, and the summation was performed over these neighboring

particles. In the definition of $\phi_6(k)$, θ_{kl} is given by

$$\theta_{kl} = \cos^{-1} \left(\frac{\mathbf{r}_{kl} \cdot \mathbf{e}_x}{|\mathbf{r}_{kl}|} \right), \quad (10)$$

where \mathbf{e}_x represents the normal vector in the x -direction. Particles forming a kagome lattice in an experiment³² were observed to each be attached to two substrate particles. Thus, the k th particle was considered to be part of the kagome lattice when it was attached to two substrate particles, had four neighbors that were attached to two substrate particles, and satisfied $\phi_6(k) > 0.7$.

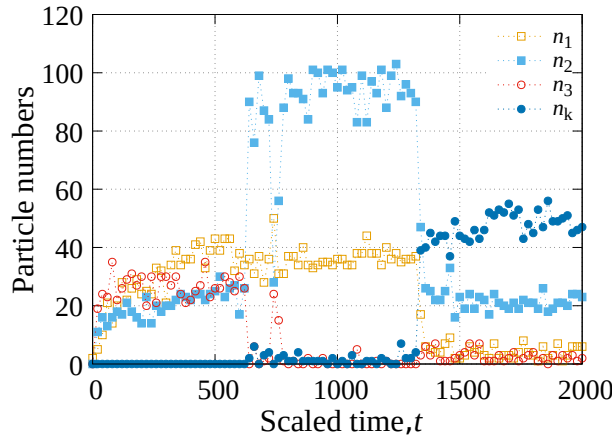


Figure 2: Time evolution of the numbers of particles attached to substrate particles during the simulation shown in Fig. 1. n_1 , n_2 , and n_3 represent the number of particles attached to one, two, and three substrate particles, respectively. When counting n_2 , the number of particles forming the kagome lattice, n_k , is excluded.

The process of kagome lattice formation. Many particles form the kagome lattice in Fig 1. To understand the formation process of the kagome lattice, we investigate how the number of particles in the kagome lattice evolved during the simulation. Figure 2 shows the time evolution of the number of particles in the kagome lattice, n_k . Additionally, this figure shows the time evolution of the numbers of particles attached to three substrate particles n_3 , to two substrate particles but not included in the kagome lattice n_2 , and to one substrate particle n_1 . In the initial stage, n_3 is larger than n_2 , and particles forming the

kagome lattice were not observed. At this stage, because the density of particles attached to the substrate was low, epitaxial particles seldom attached to each other, which means that the epitaxial particles hardly interacted with each other. Thus, the epitaxial particles preferentially attached to the sites where they could interact with three substrate particles to maximize their interaction with substrate particles. As the simulation time progressed, the density of particles on the substrate increased because of the sedimentation of particles. Once the interaction between epitaxial particles became possible, n_2 increased sharply at about $t = 6.4 \times 10^2$. The state with large n_2 remained until around $t = 1.32 \times 10^3$. In the intermediate stage ($6.4 \times 10^2 \leq t \leq 1.32 \times 10^3$), epitaxial particles attached to three substrate particles were hardly observed, although epitaxial particles attached to one substrate particle were still present. When $t = 1.34 \times 10^3$, n_1 and n_2 decreased and n_k increased suddenly. When $1.34 \times 10^3 \leq t$, particles forming the kagome lattice and ones attached to two substrate particles but not part of the kagome lattice were observed. By contrast, n_1 and n_3 were negligible.

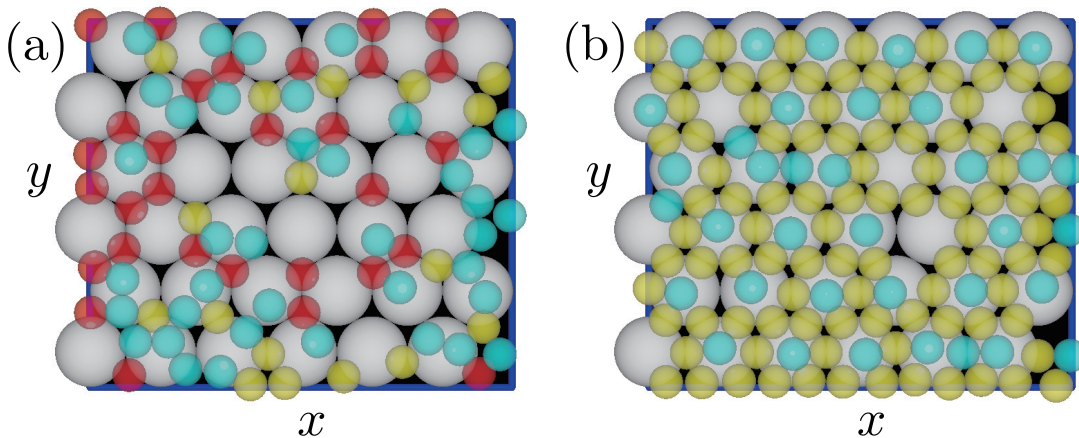


Figure 3: Snapshots of the first epitaxial layer during (a) the initial stage ($t = 600$) and (b) the middle stage ($t = 680$). The simulation parameters were as follows: $N_{\text{sub}} = 36$, $N_{\text{epi}} = 900$, $\rho = 0.02$, $2R_{\text{sub}}A/k_{\text{B}}T = 5.6$, and $\Delta t = 5.0 \times 10^{-6}$

Snapshots of the initial and middle stages. We also examined how snapshots of the first epitaxial layer evolved during the formation of the kagome lattice. Figure 3 shows

typical snapshots of the initial and middle stages. In these snapshots, particles attached to three substrate particles are shown in red and those attached to two substrate particles but not forming the kagome lattice are shown in yellow. Particles attached to one particle are depicted in cyan and those forming the kagome lattice are shown in green. In the initial stage (Fig. 3a), the density of particles on the substrate is low and particles appear to be located at random. By contrast, in the middle stage (Fig. 3b), the epitaxial particles form a hexagonal structure consisting of the particles attached to two substrate particles and those attached to one substrate particle. Considering Fig. 1, it is evident that the kagome lattice formed when the epitaxial particles attached to one substrate particle detached from the substrate.

In an experiment,³⁴ a kagome lattice was generated after honeycomb lattice formation followed by hexagonal lattice formation. Thus, the sequence of structural transitions observed in our simulation agreed with those observed experimentally. The simulations were performed using an interaction energy that was much larger than the thermal energy. Thus, we compared the internal energy gain per particle for honeycomb lattice formation with that for kagome lattice formation to investigate which structure is more stable. Because the particle size is small, epitaxial particles in the honeycomb lattice do not interact with each other, but they each interact with three substrate particles. When the epitaxial particles form an ideal honeycomb lattice, the internal energy gain per particle, $\epsilon_{\text{honeycomb}}$, is given by

$$\epsilon_{\text{honeycomb}} = 3U_0(R_{\text{sub}}, R_{\text{epi}}) = \frac{12AR_{\text{sub}}R_{\text{epi}}}{(R_{\text{sub}} + R_{\text{epi}})}. \quad (11)$$

By contrast, in the kagome lattice, an epitaxial particle interacts with two substrate particles and four neighboring epitaxial particles. Thus, the internal energy gain per particle, ϵ_{kagome} , is estimated to be

$$\epsilon_{\text{kagome}} = 2U_0(R_{\text{sub}}, R_{\text{epi}}) + 4AR_{\text{epi}} = \frac{8AR_{\text{sub}}R_{\text{epi}}}{(R_{\text{sub}} + R_{\text{epi}})} + 4AR_{\text{epi}}. \quad (12)$$

The difference between the energy gains of the two structures is given by

$$\epsilon_{\text{honeycomb}} - \epsilon_{\text{kagome}} = -\frac{4AR_{\text{sub}}R_{\text{epi}}}{(R_{\text{sub}} + R_{\text{epi}})} < 0. \quad (13)$$

The number of particles needed to form the kagome lattice is larger than that needed to generate the honeycomb lattice, and therefore the formation of the kagome lattice is favored when the density of epitaxial particles is high. The honeycomb lattice forms in the initial stage, when the density of epitaxial particles on the substrate is low. When epitaxial particles in solution settle on the substrate, the density of epitaxial particles on the substrate increases, and the honeycomb lattice transitions into the kagome lattice, which has a larger interaction energy gain when that of the honeycomb lattice.

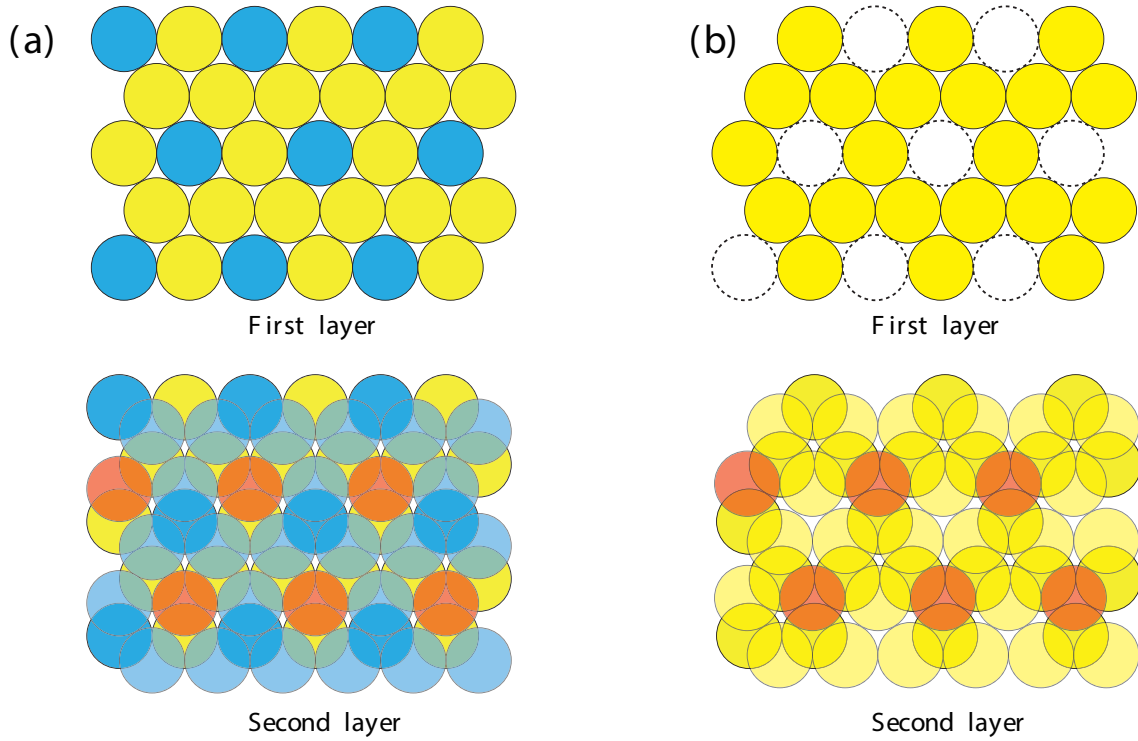


Figure 4: Schematic figures of ideal second epitaxial layers formed on the first epitaxial layers of (a) the hexagonal lattice and (b) the kagome lattice. For particles in the first layer, particles attached to one and two substrate particles are shown in blue and yellow, respectively. For particles in the second layer, particles attached to one, two, and three particles in the first layer are shown in blue, yellow, and orange, respectively.

During the transition from honeycomb lattice to kagome lattice, a hexagonal lattice is

temporarily formed. When considering only the first epitaxial layer, the transition from the hexagonal lattice to the kagome lattice appears energetically disadvantageous, because the internal energy gain decreases as a result of the loss of one epitaxial particle. However, the formation of upper layers on the kagome lattice is energetically more favorable than that on the hexagonal lattice. For simplicity, we considered the difference between the second layers on the kagome and hexagonal lattices. Figure 4 schematically illustrates the first and second ideal epitaxial layers, where the lattice constant is assumed to be $2R_{\text{epi}}$ with $R_{\text{epi}}/R_{\text{sub}} = 0.5$. The number of attracting particles is indicated by color differences. In the first epitaxial layer, all particles interact with two substrate particles in the kagome lattice (Fig. 4b). By contrast, some particles in the hexagonal lattice interact with only one substrate particle. The presence of these singly interacting particles causes the first layer in the hexagonal lattice to become uneven. This structural unevenness affects the attachment of the second layer to the first epitaxial layer. The second layer *i* in an experiment³⁴ possessed a hexagonal structure, and thus here we considered the second epitaxial layer with a hexagonal structure without the modulation of the lattice constant in the *xy* plane. Many particles in the second layer were attached to only one particle in the first epitaxial layer, although some particles attached to three first layer particles. Removal of the particles interacting with only one substrate particle from the first epitaxial layer allowed particles in the second layer to interact with two or three particles in the first epitaxial layer. Consequently, the hexagonal lattice in the first epitaxial layer transitioned into the kagome lattice to increase the energy gain when generating hexagonal upper layers.

Relationship between the formation of the kagome lattice and upper layer structure. Before and after the formation of the kagome lattice, the particle distribution in the *z*-direction changed considerably in the simulations. Figure 5 shows the distribution of epitaxial particles in the *z*-direction. The upper layer did not form before the generation of the kagome lattice (Fig. 5a). However, once the kagome lattice was produced at the first

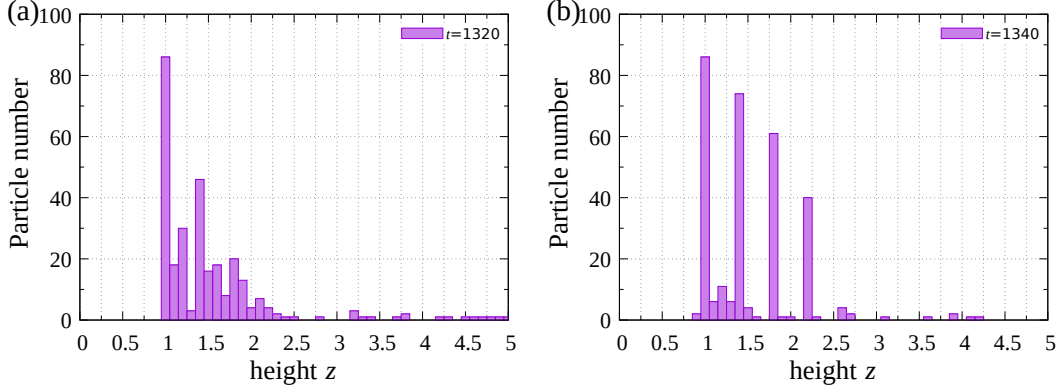


Figure 5: The distribution of particles in the z -direction (a) before ($t = 1320$) and (b) after ($t = 1340$) kagome lattice formation for Fig. 2.

epitaxial layer (Fig. 5b), not only the second layer but also much higher layers were generated at the same time.

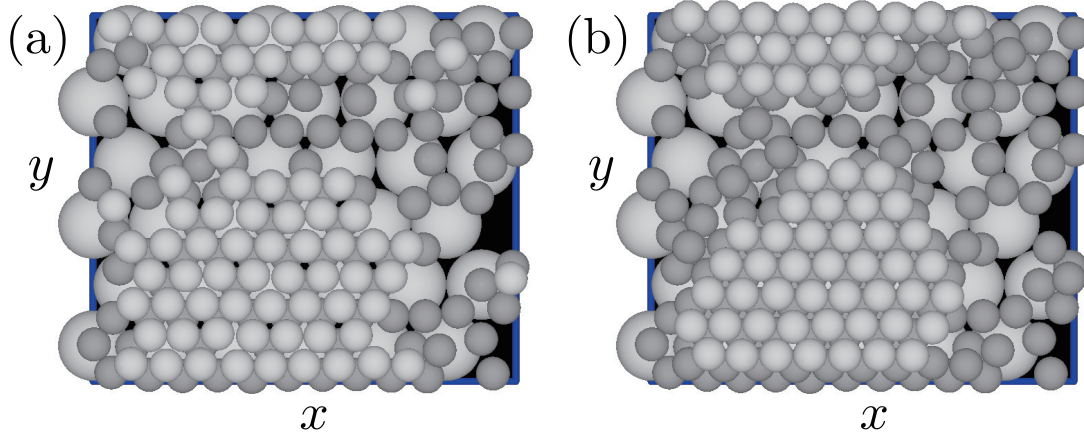


Figure 6: Snapshots of (a) the second layer and (b) the third layer at $t = 1340$. In both (a) and (b), particles in the lower epitaxial layers are shown in dark gray, whereas particles in the second and third layers are depicted in white. The simulation parameters were as follows: $N_{\text{sub}} = 36$, $N_{\text{epi}} = 900$, $\rho = 0.02$, $2R_{\text{sub}}A/k_{\text{B}}T = 5.6$, and $\Delta t = 5.0 \times 10^{-6}$

Figure 6 a and b shows the particle positions in the second and third epitaxial layers at $t = 1340$, respectively. In this figure, the particles in the top epitaxial layer are shown in white particles and those in the lower epitaxial layers are shown by dark gray. The epitaxial particles in the second and third epitaxial layers was found to form hexagonal lattices. Figure 7 shows the first and second epitaxial layers during the initial stage of kagome lattice

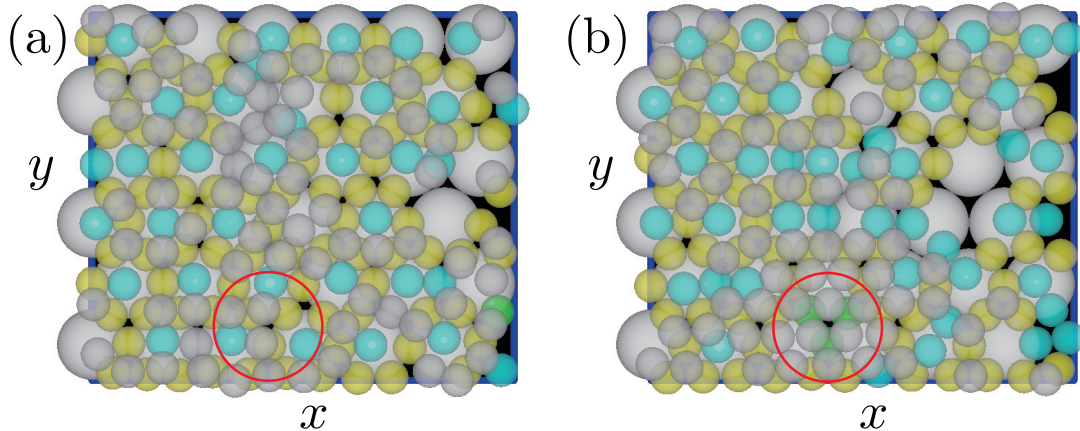


Figure 7: Snapshots of the first and second epitaxial layers (a) immediately before kagome lattice formation ($t = 1328.0$) and (b) Immediately after the start of kagome lattice formation ($t = 1329.4$). Particle colors in the first layer are the same as those in Fig. 1 and particles in the second layer are shown in gray. Particles in lower epitaxial layers are dark gray. The simulation parameters were as follows: $N_{\text{sub}} = 36$, $N_{\text{epi}} = 900$, $\rho = 0.02$, $2R_{\text{sub}}A/k_{\text{B}}T = 5.6$, and $\Delta t = 5.0 \times 10^{-6}$

formation. The particle colors in the first epitaxial layer are the same as those in Fig. 1, whereas the particles in the second epitaxial layer are shown in gray. We focus on the areas indicated by red circles. Immediately before the formation of the kagome lattice (Fig.7a), a lattice structure was not present in the second epitaxial layer. However, when the kagome lattice began to form, a hexagonal structure was locally created on the kagome lattice.

Dependence of kagome lattice formation on the interaction energy and size ratio of particles. Experimentally, it is relatively straightforward to modify the interaction strength between particles by controlling the density of polymers in the solution. It is also feasible to conduct experiments with different ratios of epitaxial particle size to substrate particle size. Thus, we investigated how the formation of the kagome lattice depended on both the interaction energy and particle size ratio. In the following, we performed 20 individual runs and report the average.

Figure 8a shows the dependence of the number of particles forming the kagome lattice on interaction energy. Because the attachment of epitaxial particles to substrate particles

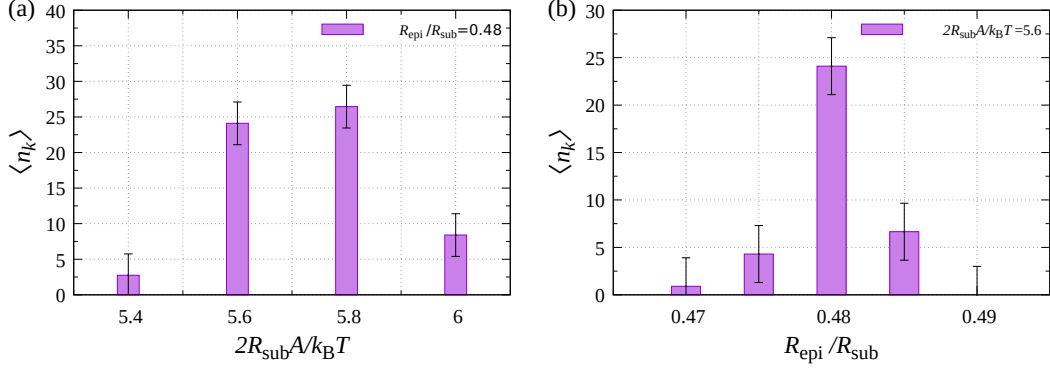


Figure 8: Dependence of the number of particles included in the kagome lattice on (a) interaction energy and (b) particle size. Data are averaged over 20 individual runs.

becomes easier with larger internal energy, the number of particles forming the kagome lattice increased with the interaction energy. However, when $2R_{\text{sub}}/k_B T = 6.0$, the interaction energy became too large and the three-dimensional nucleation in the solution was no longer negligible. The number of n_k decreased because the number of particles attached to the substrate particles became small. However, the formation of three-dimensional nuclei deviates from the experiment observation³⁴ Figure 8b shows the dependence of the number of particles forming the kagome lattice on particle size. The interaction strength decreases with particle size in Eq. (7). In addition, for smaller particles, the interaction between epitaxial particles in the kagome lattice configuration becomes weaker because the interaction is short-range. A kagome lattice such as that shown in Fig. 1 can form when $r_{\text{epi}}/r_{\text{sub}} \leq 0.5$. However, when $r_{\text{epi}}/r_{\text{sub}} \leq 0.49$, the kagome lattice was hardly generated in the simulations, which is probably because even the small fluctuation of particle positions induced by thermal fluctuations prevents the formation of the kagome lattice when the particle size approaches its upper limit.

Conclusions

Brownian dynamics simulations were conducted to examine the formation of a kagome lattice observed in an experiment.³⁴ The kagome lattice formed when $R_{\text{epi}}/R_{\text{sub}} = 0.48$, which is

consistent with the experiment results. In the simulations, when the particle density on the substrate was sufficiently large, a honeycomb lattice formed followed by the formation of a hexagonal structure. Subsequently, the particles attached to one substrate particle were incorporated into the layer, leading to the formation of a kagome lattice in the first epitaxial layer. In the experiment,³⁴ the number of epitaxial particles on the substrate increased before the formation of the kagome lattice. Thus, the simulations exhibit the same trend as the experimental observations.

The transition from the preliminary structures to the final structure appears reasonable when considering the energy gain. When we compare the honeycomb and kagome lattices, only the energy changes in the first layer need to be considered. However, for the transition from the hexagonal structure to the kagome lattice, we need to consider the ease of forming the second layer structure. Although the situation is different, a multistep process to form final structure has also been observed in a different system.⁴⁸ In both cases, the systems appear to follow a multistep pathway to lower the overall free energy of the process, rather than choosing a single-step path that needs overcoming a larger free energy barrier to overcome.

Although the simulation results successfully captured the formation process of the first epitaxial layer, a large difference remains between the simulation and experiment regarding the upper layers: a kagome lattice did not form in the upper layers in the simulations whereas it formed in the third, fourth, and sixth epitaxial layers in the experiment.³⁴ At present, we do not have an obvious explanation for this discrepancy between the simulation results and experimental observations. However, we hypothesize that strain in the heteroepitaxial layer may play an important role. In the experiment,³⁴ the lattice spacing in the epitaxial layers decreased in the upper layers, which was probably related to strain caused by the lattice mismatch between the epitaxial layer and substrate. By contrast, our simulations did not exhibit a similar pronounced decrease in the lattice spacing as the layer number increased. Nevertheless, because our model captured the essential properties of the process

of kagome lattice formation, the kagome lattice may form in the upper layer under suitable conditions. Alternatively, additional factors may need to be incorporated into the model to achieve kagome lattice formation in the upper layers. Investigating the reasons behind the differences between the experimental and simulation results in the upper layers remains an important direction for future research.

Acknowledgement

This study was supported by the Japan Society for the Promotion of Science (JSPS) KAKENHI (Grant no. JP23K03258) and the Grant for Joint Research Program of the Institute of Low Temperature Science, Hokkaido University, (Grant no. 24G032).

References

- (1) Yablonovitch, E. Inhibited spontaneous emission in solid-state physics and electronics. *Phys. Rev. Lett.* **1987**, *58*, 2059-2062.
- (2) John, S. Strong localization of photons in certain disordered dielectric superlattices. *Phys. Rev. Lett.* **1987**, *58*, 2486-2489.
- (3) Vlasov, Y. A.; Bo, X. Z.; Sturm, J. C.; Norris, D. J. On-chip natural assembly of silicon photonic bandgap crystals. *Nature* **2001**, *414*, 289-293.
- (4) Schrodén, R. C.; Al-Daous, M.; Blanford, C. F.; Stein, A. Optical properties of inverse opal photonic crystals. *Chem. Mater.* **2002**, *14*, 3305-3315.
- (5) Souslov, A.; Liu, A.; Lubensky, T.; Elasticity and Response in Nearly Isostatic Periodic Lattices. *Phys. Rev. Lett.* **2009**, *103*, 205503.
- (6) Dyogtyev, A. V.; Sukhoivanov, I. A.; De La Rue, R. M. Photonic band-gap maps for

- different two dimensionally periodic photonic crystal structures. *J. Appl. Phys.* **2010**, *107*, 013108.
- (7) Iwashita, Y.; Kimura, Y. Orientational order of one-patch colloidal particles in two dimensions. *Soft Matter* **2014**, *10*, 7170-7181.
- (8) Shin, H.; Schweizer, K. S. Theory of two-dimensional self-assembly of Janus colloids: crystallization and orientational ordering. *Soft Matter* **2014**, *10*, 262-274.
- (9) Preisler, Z.; Vissers, T.; Munaò, G.; Smallenburg, F.; Sciortino, F. Equilibrium phases of one-patch colloids with short-range attractions. *Soft Matter* **2014**, *10*, 5121-5128.
- (10) Iwashita, Y.; Kimura, Y. Spatial confinement governs orientational order in patchy particles. *Sci. Rep.* **2016**, *6*, 27599.
- (11) Preisler, Z.; Vissers, T.; Smallenburg, F.; Sciortino, F. Crystals of Janus colloids at various interaction ranges. *J. Chem. Phys.* **2016**, *145*, 064513.
- (12) Chen, Q.; Bae, S. C.; Granick, S. Directed self-assembly of a colloidal kagome lattice. *Nature* **2011**, *469*, 381-384.
- (13) Sato, M. Two-Dimensional Structures Formed by Triblock Patchy Particles with Two Different Patches. *Langmuir* **2022**, *38*, 15404-15412
- (14) Reinhart, W. F.; Panagiotopoulos, A. Z. Equilibrium crystal phases of triblock Janus colloids. *J. Chem. Phys.* **2016**, *145*, 094505.
- (15) Morpew, D.; Shaw, J.; Avins, C.; Chakrabarti, D. Programming Hierarchical Self-Assembly of Patchy Particles into Colloidal Crystals via Colloidal Molecules. *ACS Nano* **2018**, *12*, 2355-2364.
- (16) Rao, A. B.; Shaw, J.; Neophytou, A.; Morpew, D.; Sciortino, F.; Jhonston, R. L.; Chakrabarti, D. Leveraging Hierarchical Self-Assembly Pathways for Realizing Colloidal Photonic Crystals. *ACS Nano* **2020**, *14*, 5348-5359.

- (17) Neophytou, A.; Manoharan, V. N.; Chakrabarti, D. Self-Assembly of Patchy Colloidal Rods into Photonic Crystals Robust to Stacking Faults. *ACS Nano* **2021**, *15*, 2668-2678.
- (18) Xu, H.; Baus, M. Freezing in the presence of a periodic external potential. *Physics Letters A* **1986**, *117*, 127-131.
- (19) van Blaaderen, A.; Ruelt, R.; Wiltzius, P. Template-directed colloidal crystallization. *Nature* **1997**, *385*, 321-324.
- (20) Cheng Z., Russel W. B., Chaikin P. M., Controlled growth of hard-sphere colloidal crystals. *Nature* **1999**, *401*, 893.
- (21) Hoogenboom, J. P.; Yethiraj, A.; van Langen-Suurling, A. K.; Romijn, J.; van Blaaderen, A. Epitaxial crystal growth of charged colloids. *Phys. Rev. Lett.* **2002**, *89*, 256104.
- (22) Reichhardt, C.; Olson, C. J. Novel Colloidal Crystalline States on Two-Dimensional Periodic Substrates. *Phys. Rev. Lett.* **2002**, *88*, 248301.
- (23) Schall P.; Cohen I.; Weitz D. A.; Spaepen F. Visualization of dislocation dynamics in colloidal crystals. *Science* **2004**, *305*, 1944.
- (24) Hynninen, A-P.; Thijssen, J. H. J.; Vermolen, E. C. M.; Dijkstra, M.; van Blaaderen, A. Self-assembly route for photonic crystals with a bandgap in the visible region *Nat. Mater.* **2007**, *6*, 202-205.
- (25) Bechinger, C.; Frey, E. *Colloids on Patterned Substrates*; Wiley, 2007.
- (26) Shawish, S. El; Dobnikar, J.; Trizac, E. Ground states of colloidal molecular crystals on periodic substrates. *Soft Matter* **2008**, *4*, 1491-1498.
- (27) Ganapathy, R.; Buckley, M. R.; Gerbode, S. J.; Cohen, I. Direct measurements of island growth and step-edge barriers in colloidal epitaxy. *Science* **2010**, *327*, 445-448.

- (28) Allahyarov, E.; Sandomirski, K.; Egelhaaf, S.U.; Löwen, H. Crystallization seeds favour crystallization only during initial growth, *Nat. Commun.* **2015**, *6*, 7110.
- (29) Dasgupta, T.; Edison, J. R.; Dijkstra, M. Growth of defect-free colloidal hard-sphere crystals using colloidal epitaxy. *J. Chem. Phys.* **2017**, *146*, 074903.
- (30) Mondal, M.; Mishra, C. K.; Banerjee, R.; Narasimhan, S.; Sood, A. K.; Ganapathy, R. Cooperative particle rearrangements facilitate the self-organized growth of colloidal crystal arrays on strain-relief patterns. *Sci. Adv.* **2020**, *6*, 8418.
- (31) Mondal, M.; Ganapathy, R. Direct Measurements of Surface Strain-Mediated Lateral Interactions between Adsorbates in Colloidal Heteroepitaxy. *Phys. Rev. Lett.* **2022**, *129*, 088003.
- (32) Nozawa, J.; Uda, S.; Toyotama, A.; Yamanaka, J.; Niinomi, J.; Okada, J. Heteroepitaxial fabrication of binary colloidal crystals by a balance of interparticle interaction and lattice spacing. *J. Colloid Interface Sci.* **2022**, *608*, 873-881.
- (33) Nozawa, J.; Uda, S.; Niinomi, J.; Okada, J.; Fujiwara, K. Heteroepitaxial Growth of Colloidal Crystals: Dependence of the Growth Mode on the Interparticle Interactions and Lattice Spacing. *J. Phys. Chem. Lett.* **2022**, *13*, 6995-7000.
- (34) Nozawa, J.; Sato, M.; Uda, S.; Fujiwara, K. Multi-layer kagome lattices assembled with isotropic spherical colloids via heteroepitaxial growth, *Colloids Interface Sci. Commun.* **2025**, *64*, 100815.
- (35) Sato, M.: Formation of various structures caused by particle size difference in colloidal heteroepitaxy *Sci. Reps.* **2024**, *14*, 3245.
- (36) Sato, M.: Structures of the First Epitaxial Layer Created in Colloidal Heteroepitaxy. *J. Phys. Chem. B* **2024**, *128*, 1077910787.

- (37) Edlund, E.; Lindgren, O.; N. Jacobi, M.: Designing isotropic interactions for self-assembly of complex lattices. *Phys. Rev. Lett.* **2011**, *107*, 085503.
- (38) D. Batten, R.; A. Huse, D.; H. Stillinger, F.; Torquato, S.: Novel ground-state crystals with controlled vacancy concentrations: from kagome to honeycomb to stripes, *Soft Matter* **2011**, *7*, 61946204.
- (39) Baumketner, A.; Melnyk, R.: Kagome lattice made by impenetrable ellipses with attractive walls. *Soft Matter* **2022**, *18*, 38013814.
- (40) Baumketner, A.: Self-assembly of two-dimensional lattices driven by shape complementarity and attractive interactions, *J. Mol. Liq.* **2023**, *386*, 122526.
- (41) Asakura, S.; Oosawa, F. On Interaction between Two Bodies Immersed in a Solution of Macromolecules. *J. Chem. Phys.* **1954**, *22*, 1255-1256.
- (42) Vrij, A. Polymers at Interfaces and the Interactions in Colloidal Dispersions. *Pure Appl. Chem.* **1976** *48*, 471-483.
- (43) Ermark, D. L; A computer simulation of charged particles in solution. I. Technique and equilibrium properties. *J. Chem. Phys.* **1975**, *62*, 4189-4195.
- (44) Lekkerkerker, H. N. W.; Tuinier, R. *Colloids and the Depletion Interaction*; Springer: Netherlands, 2011; Chapter 1.
- (45) Guo, S.; Nozawa, J.; Hu, S.; Koizumi, H.; Okaza, J.; Uda, S. Heterogeneous Nucleation of Colloidal Crystals on a Glass Substrate with Depletion Attraction. *Langmuir*, **2017**, *33*, 10543-10549.
- (46) Toyotama, A.; Okuzono, T.; Yamanaka, J. Spontaneous Formation of Eutectic Crystal Structures in Binary and Ternary Charged Colloids due to Depletion Attraction. *Sci. Rep.* **2016**, *6*, 1255-1256.

- (47) Morse, P. M. Diatomic molecules according to the wave mechanics. II. Vibrational levels. **1929**, *Phys. Rev.* *34*, 57-64.
- (48) Eslami, H.; Müller-Plathe, F. Self-Assembly Pathways of Triblock Janus Particles into 3D Open Lattices. **2024**, *Small* *19*, 230737.

TOC Graphic

